Dalton Transactions

ROYAL SOCIETY OF CHEMISTRY

PAPER

View Article Online
View Journal | View Issue

Cite this: *Dalton Trans.*, 2024, **53**, 6031

Synthesis and preclinical evaluation of BOLD-100 radiolabeled with ruthenium-97 and ruthenium-103†

B. Happl,[a,b,c] T. Balber,[a,b,d] P. Heffeter,[e,f] C. Denk,[g,h] J. M. Welch,[h] U. Köster,[i] C. Alliot,[j,k] A.-C. Bonraisin,[j] M. Brandt,[a,b,d] F. Haddad,[j,l] J. H. Sterba,[h] W. Kandioller,[c,f] M. Mitterhauser,[a,b,c,d] M. Hacker,[b] B. K. Keppler[c,f] and T. L. Mindt *[a,b,c,d]

Received 14th January 2024,
Accepted 26th February 2024

DOI: 10.1039/d4dt00118d

rsc.li/dalton

BOLD-100 (formerly IT-139, KP1339), a well-established chemotherapeutic agent, is currently being investigated in clinical trials for the treatment of gastric, pancreatic, colorectal, and bile duct cancer. Despite numerous studies, the exact mode of action is still the subject of discussions. Radiolabeled BOLD-100 could be a powerful tool to clarify pharmacokinetic pathways of the compound and to predict therapy responses in patients using nuclear molecular imaging prior to the therapy. In this study, the radiosyntheses of carrier-added (c.a.) [$^{97/103}$Ru]BOLD-100 were performed with the two ruthenium isotopes ruthenium-103 (^{103}Ru; β^-, γ) and ruthenium-97 (^{97}Ru; EC, γ), of which in particular the latter isotope is suitable for imaging by single-photon emission computed tomography (SPECT). To identify the best tumor-to-background ratio for diagnostic imaging, biodistribution studies were performed with two different injected doses of c.a. [^{103}Ru]BOLD-100 (3 and 30 mg kg^{-1}) in Balb/c mice bearing CT26 allografts over a time period of 72 h. Additionally, *ex vivo* autoradiography of the tumors (24 h p.i.) was conducted. Our results indicate that the higher injected dose (30 mg kg^{-1}) leads to more unspecific accumulation of the compound in non-targeted tissue, which is likely due to an overload of the albumin transport system. It was also shown that lower amounts of injected c.a. [^{103}Ru]BOLD-100 resulted in a relatively higher tumor uptake and, therefore, a better tumor-to-background ratio, which are encouraging results for future imaging studies using c.a. [^{97}Ru]BOLD-100.

1. Introduction

Radiolabeling of chemotherapeutic agents with radiometals was already performed in the 1970s with platinum compounds, such as cisplatin using platinum-195 m.[1] The lack of commercial availability of other suitable radiometals and the sometimes complex or multi-step synthetic procedures, are the main reasons why examples of radiolabeling studies of metal-based chemotherapeutic agents are relatively scarce. Aside from platinum compounds, one of the most promising ruthenium(III) anticancer complexes is BOLD-100 (formerly IT-139 or KP1339, Fig. 1), which is currently undergoing clinical investigation.[2,3] The exact mode of action of BOLD-100 and the underlying mechanisms of its cytotoxic effects are still not fully characterized. Several studies report on the binding of the Ru(III) complex to blood proteins, such as albumin, in a first step.[4–6] This is followed by the reduction of the prodrug to an active Ru(II) species within the hypoxic tumor environment,[7] in which the albumin–Ru conjugate is accumulated by the enhanced permeability and retention effect.[8,9] *In vitro* studies have shown that BOLD-100 induces endoplasmic reticulum stress in combination with down-regulation of the glucose-

[a]*Ludwig Boltzmann Institute Applied Diagnostics, General Hospital of Vienna, Währinger Gürtel 18-20, 1090 Vienna, Austria. E-mail: thomas.mindt@univie.ac.at*
[b]*Division of Nuclear Medicine, Department of Biomedical Imaging and Image Guided Therapy, Medical University of Vienna, Währinger Gürtel 18-20, 1090 Vienna, Austria*
[c]*Institute of Inorganic Chemistry, Faculty of Chemistry, University of Vienna, Josef-Holaubek-Platz 2 and Währinger Straße 42, 1090 Vienna, Austria*
[d]*Joint Applied Medicinal Radiochemistry Facility of the University of Vienna and the Medical University of Vienna, Vienna, Austria*
[e]*Center for Cancer Research and Comprehensive Cancer Center, Medical University of Vienna, Borschkegasse 8A, 1090 Vienna, Austria*
[f]*Research cluster "Translational Cancer Therapy Research", Währinger Straße 42, 1090 Vienna, Austria*
[g]*Institute of Applied Synthetic Chemistry, Technische Universität (TU) Wien, Getreidemarkt 9, 1060 Vienna, Austria*
[h]*Center for Labelling and Isotope Production, TRIGA Center Atominstitut, TU Wien, Vienna, Austria*
[i]*Institut Laue-Langevin, 71 avenue des Martyrs, 38042 Grenoble Cedex 9, France*
[j]*GIP ARRONAX, 1 rue Aronnax, CS10112, 44817 Saint-Herblain Cedex, France*
[k]*CRCI2NA, Inserm/CNRS/Nantes Université, 8 quai Moncousu, 44007 Nantes Cedex 1, France*
[l]*Laboratoire Subatech, UMR 6457, IMT Nantes Atlantique/CNRS-IN2P3/Nantes Université, 4 Rue A. Kastler, BP 20722, 44307 Nantes Cedex 3, France*
† Electronic supplementary information (ESI) available. See DOI: https://doi.org/10.1039/d4dt00118d

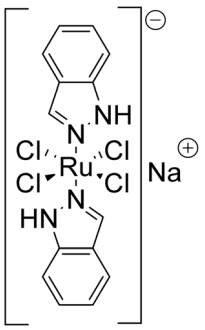

Fig. 1 The clinically studied ruthenium(III) complex BOLD-100.

regulated protein (GRP78),[10,11] and apoptotic effects that were demonstrated in 2D and 3D cell culture assays.[12–14] The induction of reactive oxygen species[15] and the triggering of immunogenic cell death[16] are alternative pathways reported for the anticancer activity of BOLD-100. Recently, BOLD-100 has been shown to target directly the onco-metabolism by inhibiting glycolysis, downregulating lactate release, and altering epigenetic gene expression *via* interaction with histone acetylation.[17] Still, multiple studies have been and are being conducted to evaluate the mode of action in detail.[18,19] Nevertheless, after a dose escalation clinical phase I study,[20] BOLD-100 is currently undergoing phase Ib/IIa trials in combination with FOLFOX for the treatment of gastric, pancreatic, colorectal, and bile duct cancer (NCT04421820).[21] The first results of this study have shown that this combination represents a well-tolerated treatment in heavily pre-treated stage IV biliary tract and gastric cancer patients,[22] as well as in pre-treated advanced colorectal cancer parients.[23]

Despite all the new insights into the mode of action of BOLD-100 obtained by various studies in the recent past,[17–19] the radiolabeling of BOLD-100 is of great interest. A radiolabeled version of BOLD-100 would not only facilitate biodistribution experiments of the drug for the assessment of its pharmacokinetic and pharmacodynamic properties, but also enable diagnostic imaging such as single-photon emission computed tomography (SPECT) to predict the therapy response in a personalized medicine approach. In this context, the radiolabeling of BOLD-100 without any structural modifications made possible by the employment of radioactive ruthenium isotopes would be the best choice, because the biological properties of the drug should remain unchanged. Although the medical relevance of ruthenium-97 (^{97}Ru) and ruthenium-103 (^{103}Ru) was already discussed in 1970 [24] and 1981,[25] there are only few literature reports on radioactive ruthenium complexes and preclinical studies thereof in the last decades. This is likely the result of the limited commercial availability of these radionuclides, whose large-scale production is not yet established. The β^- emitter ^{103}Ru can be produced by the irradiation of natural ruthenium (^{nat}Ru, composition: ^{96}Ru (5.54%), ^{98}Ru (1.87%), ^{99}Ru (12.76%), ^{100}Ru (12.60%), ^{101}Ru (17.06%), ^{102}Ru (31.55%), and ^{104}Ru (18.62%)) or of enriched ^{102}Ru with thermal neutrons *via* the ^{102}Ru(n, γ)^{103}Ru reaction.[26,27] ^{97}Ru can be produced by alpha particle induced nuclear reaction on natural molybdenum (^{nat}Mo) *via* ^{nat}Mo(α, xn)^{97}Ru,[28,29] by the irradiation of enriched ^{96}Ru with thermal neutrons *via* the ^{96}Ru(n, γ)^{97}Ru reaction or by proton irradiation of long-lived technetium-99 (^{99}Tc) *via* ^{99}Tc(p, 3n)^{97}Ru reaction.[30] ^{97}Ru decays by 100% electron capture, releasing photons with energies of 216 keV (86%) and 324 keV (11%), the former of which is within the energy window of clinical SPECT detectors. Additionally, the two ruthenium isotopes (^{97}Ru and ^{103}Ru) could represent a possible theragnostic pair, the first for SPECT imaging and the latter for therapy (Table 1).[31,32]

In a previous study, we reported that the radiolabeling of BOLD-100 with ^{103}Ru did not affect the biological behavior because the biodistributions of both radioactive and non-radioactive compounds were similar.[34] However, due to limitations of the analytical method used for the non-radioactive complex (inductively coupled plasma mass spectrometry (ICP-MS)), the administered amount of drug was quite high (30 mg kg^{-1}, 1.2 μmol per mouse) and above the molar amount of mouse serum albumin (MSA; approx. 0.3–0.4 μmol per mouse).[35] We hypothesized that blood proteins, which are supposed to be the main transporters of BOLD-100,[36] were overloaded with the drug in these first experiments. As a result, some of the injected BOLD-100 remained unbound in serum that in turn effected a higher and unspecific uptake in various organs, such as the liver or kidneys. In an effort to lower the uptake in organs and tissue other than the tumor, we here investigated the effect of lowering the applied dose of c.a. [^{103}Ru]BOLD-100 on the biodistribution of the drug. Furthermore, to find a suitable timepoint for future imaging studies with c.a. [^{97}Ru]BOLD-100, we aimed to obtain a better tumor-to-background ratio with a lower applied dose of c.a. [^{103}Ru]BOLD-100.

Consequently, we radiolabeled BOLD-100 with c.a. ^{103}Ru and c.a. ^{97}Ru. Due to the availability of higher effective specific activities and its longer half-life, the low-amount biodistribution study was performed with c.a. [^{103}Ru]BOLD-100. Furthermore, autoradiography was performed with CT26 tumors (24 h p.i.) to examine the heterogeneity of the drug uptake.

2. Results and discussion

Production of ^{97}Ru

^{97}Ru was produced by irradiation of ^{nat}Mo foil with α particles for approximately 10 h, resulting in >300 MBq at the end of the irradiation (EOI). The target foil was dissolved and bulk Mo from the target was separated by two subsequent ion exchange columns, from which ^{97}Ru was obtained in the eluate. The final ^{97}Ru solution contained impurities of molybdenum (0.9–2.0 μg) and minor radioactive impurities in the form of ^{95}Ru ($t_{1/2}$ = 1.6 h), ^{95m}Tc ($t_{1/2}$ = 61 d), and ^{95}Tc ($t_{1/2}$ = 20.0 h) (see ESI, Fig. S1†). The radiochemical yield of ^{97}Ru was 40–56%, resulting in deliverable activities of 87–123 MBq

Table 1 Physical properties of ^{103}Ru, ^{97}Ru and clinically used ^{111}In.[33]

Nuclide	Half-life [days]	Decay mode	Energy [keV] (intensity)	Use
^{103}Ru	39.3	β^- (100%)	$E_{\beta^-,\,max}$ = 227 (92%), 113 (7%) E_γ = 497 (91%), 610 (6%)	Therapy
^{97}Ru	2.9	EC (100%)	E_γ = 216 (86%), 324 (11%)	SPECT imaging
^{111}In	2.8	EC (100%)	E_γ = 171 (91%), 245 (94%)	SPECT imaging

(74–106 MBq mL^{-1}). Due to the remaining amount of molybdenum and the modest recovery yield, the target workup process is currently being optimized.

Production of ^{103}Ru

^{nat}Ru metal foils were enclosed in quartz ampoules and irradiated in a thermal neutron flux of (5–10) × 10^{14} n cm^{-2} s^{-1} for 6–8 days, leading to activities up to 1049 MBq at the EOI. After the decay of shorter-lived nuclides, such as ^{105}Ru ($t_{1/2}$ = 4.4 h), ^{105}Rh ($t_{1/2}$ = 35.3 h) and ^{97}Ru ($t_{1/2}$ = 2.8 d), the target was dissolved in alkaline, aqueous NaOCl, then the mixture was quenched with concentrated HCl. c.a. ^{103}Ru was obtained in radiochemical yields of 81–82% (up to 648 MBq), molar activities up to 19.4 MBq μmol^{-1} (249 MBq mL^{-1}), and a radionuclide purity of >99.9% (ESI, Fig. S2†). This production method of ^{103}Ru enabled us to perform radiosyntheses with high activities that enabled biodistribution studies with lower amounts of the injected drug. In order to avoid co-production of ^{35}S and ^{36}Cl radionuclides, the production of ^{103}Ru was performed by irradiation of ^{nat}Ru metal instead of previously used ^{nat}RuCl$_3$ powder.[34]

Synthesis

The three-step synthesis of radiolabeled BOLD-100 was performed as previously published (Scheme 1).[34] c.a. [^{103}Ru]RuCl$_3$ (0.6–3.0 MBq μmol^{-1}) and c.a. [^{97}Ru]RuCl$_3$ (0.2–0.5 MBq μmol^{-1}) were employed for the preparation of radiolabeled BOLD-100. In brief, either [^{97}Ru]RuCl$_3$ or [^{103}Ru]RuCl$_3$ was refluxed in HCl (37%) and ethanol, to ensure the absence of Ru(IV) species,[37] and then reacted with indazole at elevated temperatures. The obtained indazolium complexes **1a** and **1b** were converted at room temperature (RT) into the corresponding cesium salts **2a** and **2b** upon treatment with an excess of cesium chloride. The cation exchange from cesium to sodium was performed in an aqueous solution of sodium aluminum sulfate. Pure products **3a** and **3b** were obtained by precipitation from acetonitrile/methyl *tert*-butyl ether. The yields, based on the initial amount of radioactive RuCl$_3$, were good, ranging from 61% (**1a**) and 90% (**1b**) for the indazole salt, to 55% (**2a**) and 78% (**2b**) for the cesium salt, and for the final product, 8% (**3a**) and 35% (**3b**), respectively. All complexes were characterized by RP-HPLC chromatography (see the ESI†) and the radiochemical purity of compounds **1a–3a** and **1b–3b** was >99%. The overall radiochemical yield was 8% for **3a** and 35% for **3b**, whereas the overall chemical yield determined by the weight of isolated intermediates and products was 13% for **3a** and 39% for **3b**. Specific activities at the end of synthesis ranged from 0.1 MBq mg^{-1} for **3a** to 4.1 MBq mg^{-1} for **3b**, which translates into a distinctly higher molar activity of **3b** (2.1 MBq μmol^{-1}) than of **3a** (0.05 MBq μmol^{-1}).

The differences in the final radiochemical yields of the two radionuclides might be explained by the use of different target materials and workup procedures. Presumably, the target workup and chemical separation of ^{97}Ru from the bulk material needs to be improved to obtain higher radiochemical yields of the synthesis of c.a. [^{97}Ru]BOLD-100.

However, the overall chemical yield of c.a. [^{97}Ru]BOLD-100 could be increased by a longer reaction time in the first step,

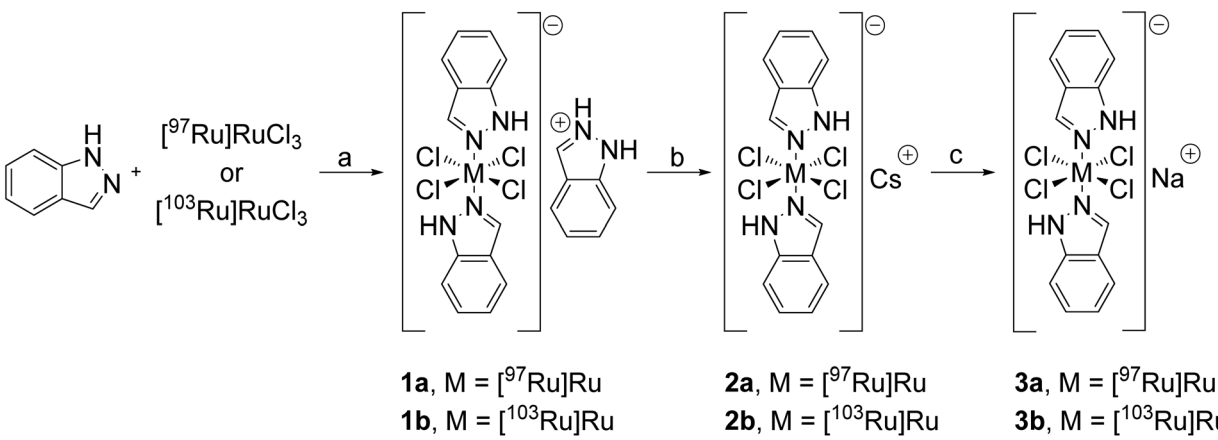

Scheme 1 Synthetic route for **3a** (*ca.* [^{97}Ru]BOLD-100) and **3b** (*ca.* [^{103}Ru]BOLD-100). (a) HCl (37%), ethanol, reflux, and 3 h; (b) CsCl, ethanol, RT, and 2 h; and (c) CsCl, aq. NaAl(SO$_4$)$_2$ (1.1 M), RT, and 24 h.

from 13% to 33% for the radiolabeling with ^{97}Ru, which is comparable to the radiolabeling results of ^{103}Ru (39%). In particular, the specific activity of ^{97}Ru needs to be increased, because the shorter half-life (2.9 days) also needs to be taken into consideration. Since the multi-step synthesis of BOLD-100 takes about three days, half of the initial activity is already decayed during the synthesis. Although we have shown that the radiolabeling of BOLD-100 with ^{97}Ru is possible, the radiochemical yield and the specific activity are currently being improved in order to allow for SPECT imaging with c.a. [^{97}Ru]BOLD-100 in the future.

Biodistribution experiments

The tissue distribution of c.a. [^{103}Ru]BOLD-100 (**3b**) was studied in female Balb/c mice bearing CT26 allografts over a time period of 72 h. Additionally, blood samples were taken *via* the facial vein 5 min and 30 min post injection (p.i.).

Blood proteins are the main transporters of BOLD-100[36] and in a study from 2016, it was shown by X-ray and ICP-MS analysis that on average approx. 1.7 moles of BOLD-100, and therefore Ru, are bound per mole of human serum albumin.[5] As in a previous study, in which the applied molar amount of drug was much higher than the molar amount of MSA,[34] we designed an experimental setup in which c.a. [^{103}Ru]BOLD-100 was injected in sub-equimolar amounts relative to MSA (a reduction by a factor of 10; 3 mg kg^{-1}, 0.1 μmol per mouse). In this concentration regime of radiolabeled BOLD-100, we expected a general reduction of unspecific uptake of radioactivity in organs such as the kidneys and the liver, which are reported to be the excretion and clearance organs.[34] To examine the overload of blood proteins, a blood sample analysis (5 and 30 min p.i.) was also performed and compared with experiments using the higher injected amount of c.a. [^{103}Ru]BOLD-100 (30 mg kg^{-1}, 1.2 μmol per mouse). Additionally, we aimed at the identification of the time point with the most appropriate tumor-to-background ratio for future SPECT imaging studies utilizing c.a. [^{97}Ru]BOLD-100.

Fig. 2 shows the amounts of ^{103}Ru accumulated in selected organs for the lower dose (3 mg kg^{-1}) and a comparison with the results of previous biodistribution experiments applying the higher dose of **3b** (30 mg kg^{-1}).[34] Blood clearance data can be found in Table 2 and selected tumor-to-organ ratios are provided in Table 3. The data for all organs and the calculated tumor-to-organ ratios can be found in the ESI (Fig. S15–S18, Tables S1–S2†).

As BOLD-100 binds to blood proteins such as albumin in the first step,[4] it was not surprising that the highest uptake of **3b** was found in the blood serum within 24 h, which also reflects the biological half-life of albumin in mice ($t_{1/2\ \mathrm{biol.}}$ = 1.2 days)[38] (Fig. 2, Table 2). Interestingly, at all studied time points, the relative amount of the circulating radioactivity in the blood serum was significantly higher for the 3 mg kg^{-1} injection compared to the 30 mg kg^{-1} dose (Table 2 and ESI, Table S1†). However, it should be noted that within the first 30 min, the blood clearance of radioactivity was faster for the lower dose of **3b** (3 mg kg^{-1}) while the level of radioactivity stayed nearly constant for the high amount injection (30 mg kg^{-1}). The slower blood clearance of the high amount injection could be an indi-

Table 2 Blood clearance of **3b** (c.a. [^{103}Ru]BOLD-100) in Balb/c mice bearing CT26 allografts over 24 h with injected amounts of 3 and 30 mg kg^{-1}. Values are means ± standard deviations of $n \geq 4$ per time point. %ID g^{-1} = percent injected dose of ^{103}Ru per gram tissue

Tissue	5 min	30 min	4 h	24 h
%ID g^{-1} tissue of c.a. [^{103}Ru]BOLD-100 (3 mg kg^{-1})				
Serum	97.22 ± 42.39	88.21 ± 7.37	44.17 ± 6.90	20.82 ± 2.51
Blood cells	20.66 ± 0.60	16.87 ± 4.56	12.82 ± 3.81	5.39 ± 1.61
%ID g^{-1} tissue of c.a. [^{103}Ru]BOLD-100 (30 mg kg^{-1})				
Serum	54.32 ± 4.85	55.39 ± 8.46	29.22 ± 4.56	11.01 ± 4.54
Blood cells	17.91 ± 3.41	15.39 ± 2.05	10.90 ± 1.94	4.67 ± 1.66

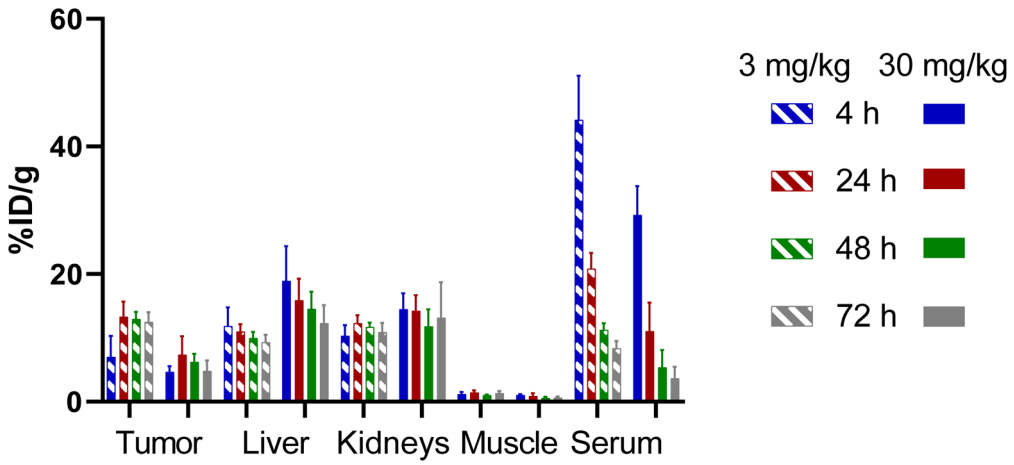

Fig. 2 Tissue distribution of the high and low doses of compound **3b** (c.a. [^{103}Ru]BOLD-100) in selected organs (%ID of ^{103}Ru g^{-1} tissue). Values are means, and error bars represent standard deviations of $n \geq 3$ per time point. Values of biodistribution experiments 4–72 h p.i. with 30 mg kg^{-1} were previously published and are included for comparison.[34] For the data of all organs see the ESI (Fig. S15–S18, Table S1†).

Table 3 Tumor-to-organ ratio of selected organs for the high and low dose application of **3b** (c.a. [^{103}Ru]BOLD-100). Values are means ± standard deviations with $n \geq 3$ per time point. Values of 30 mg kg^{-1} are included for comparison and slight variations from previously published ones can be ascribed to additionally obtained data.[34] For the data of all tumor-to-organ ratios see the ESI, Table S2†

Organ	4 h	24 h	48 h	72 h
Tumor/organ ratio of c.a. [^{103}Ru]BOLD-100 (3 mg kg^{-1})				
Liver	0.6 ± 0.1	1.2 ± 0.2	1.3 ± 0.2	1.3 ± 0.1
Kidneys	0.9 ± 0.3	1.2 ± 0.2	1.1 ± 0.1	1.1 ± 0.0
Muscle	6.9 ± 3.3	11.5 ± 1.3	12.9 ± 2.2	9.8 ± 1.6
Serum	0.2 ± 0.1	0.7 ± 0.1	1.2 ± 0.1	1.5 ± 0.1
Tumor/organ ratio of c.a. [^{103}Ru]BOLD-100 (30 mg kg^{-1})				
Liver	0.2 ± 0.2	0.5 ± 0.1	0.4 ± 0.1	0.4 ± 0.1
Kidneys	0.4 ± 0.1	0.5 ± 0.1	0.5 ± 0.1	0.4 ± 0.2
Muscle	4.4 ± 1.4	11.4 ± 1.8	10.6 ± 1.4	7.6 ± 2.4
Serum	0.2 ± 0.0	0.8 ± 0.1	1.3 ± 0.4	1.4 ± 0.3

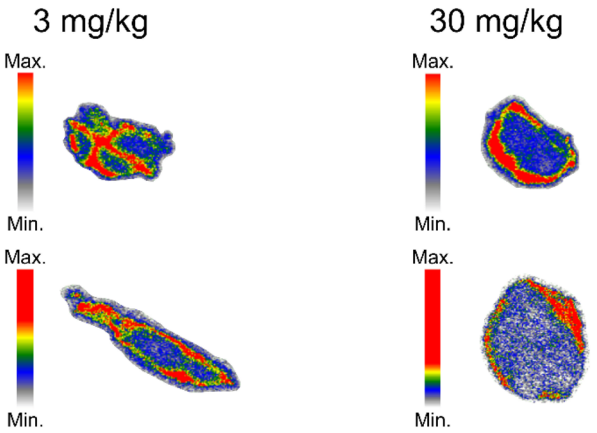

Fig. 3 Autoradiography results of tumor sections of four different CT26 tumors. Red colors indicate high ^{103}Ru uptake, and blue colors indicate low ^{103}Ru uptake.

cation for the overload of blood proteins because the bound drug can circulate for a longer time in the blood, whereas the free/unbound drug can accumulate unspecifically in tissue.

Despite the high serum uptake, the relative tumor uptake of **3b** was also increased for the low amount injection (3 mg kg^{-1}) at all studied time points (Fig. 2, ESI Table S1†). The highest tumor uptake of **3b** was found 24 h p.i. and, in contrast to the high amount injection, the radioactivity decreased only slowly and stayed nearly constant from 24 h to 72 h at approx. 13% ID g^{-1}. This result is also important for potential radionuclide therapy because the clearance from the tumor seems slower for doses that are sub-equimolar with respect to albumin. Furthermore, the relative uptake of **3b** in the liver and kidneys was slightly decreased for the low amount injection but it was still significant, which indicates unspecific uptake of **3b** in these organs, especially in the kidneys (Fig. 2, ESI Table S1†). For organs with high blood flow, such as the heart or lung, the relative amount of radioactivity was almost the same for both injected doses (ESI, Table S1†). Slightly higher uptake at some time points for the low amount injection could be explained by the higher radioactivity in serum and blood cells because these organs were not sluiced out after harvesting. In most other organs, such as the stomach, pancreas, or colon, the relative amount of radioactivity was low and did not change significantly over time. Thus, the tumor-to-organ ratios remained almost constant.

To obtain suitable differentiation of the tumor from the background and surrounding tissue in diagnostic imaging studies, a high tumor-to-organ ratio is needed. Looking at the tumor-to-organ ratios of this study, there is clearly an improvement recognizable for the low amount injection of **3b**. The relatively higher tumor uptake of radioactivity in the low amount injection experiments led to increased tumor-to-organ ratios for nearly all organs at all investigated time points in comparison with the high amount injection. The best tumor-to-background ratios were obtained 48 h and 72 h p.i. (Table 3, ESI Table S2†). Presumably, this ratio could be further increased when even lower or trace amounts of radiolabeled BOLD-100 are administered, or when later time points than 72 h are evaluated. Studies investigating the effect of further decreased amounts of applied radioactive BOLD-100 are currently ongoing.

To conclude, sub-equimolar amounts of c.a. [^{103}Ru]BOLD-100 to albumin resulted in a relative higher and prolonged tumor uptake of over 72 h, which is beneficial for therapeutic applications. Furthermore, this led to better tumor-to-background ratios at 48 h and 72 h, which is encouraging for future diagnostic SPECT imaging studies with c.a. [^{97}Ru]BOLD-100.

Autoradiography

The phenomenon of tumor heterogeneity is already known and has been studied for a long time.[39,40] It can be visualized *in vitro*, *in vivo*, or *ex vivo* by multiple techniques, including, for example, SPECT imaging.[41] Here, *ex vivo* autoradiography was implemented to prove the heterogeneous uptake of c.a. [^{103}Ru]BOLD-100 in tumor tissue. Two tumors per group (3 mg kg^{-1} and 30 mg kg^{-1}, 24 h p.i.) were cut into slices and analyzed using a phosphor imaging reader. As shown in Fig. 3, a high uptake of ^{103}Ru in the rim of the tumor was detected in all cases, whereas lower ^{103}Ru uptake was found in the tumor core. These findings are in good agreement with the studied morphology of CT26 tumors in Balb/c mice.[42] The lower uptake of radioactivity in the tumor core can be explained by damaged vascularization in this necrotic region in the tumor. These results underline once again that the analysis of the whole tumor is necessary for obtaining meaningful values for the exact uptake throughout the tumor. This is because for some analytical methods, such as ICP-MS analysis, only small parts of the tumor are usually used for analysis of content.

3. Conclusion

After the radiolabeling of BOLD-100 with c.a. ^{97}Ru and c.a. ^{103}Ru, an *in vivo* comparison of two different injected doses of

c.a. [^{103}Ru]BOLD-100 gave new insights into the biodistribution of the compound. A faster blood clearance was found for the lower injected dose of c.a. [^{103}Ru]BOLD-100 at early time points; however, the level of radioactivity in the blood was much higher over 72 h than for the higher injected dose. The relative tumor uptake was found increased for the lower dose of c.a. [^{103}Ru]BOLD-100, while the liver and kidney uptake were decreased. In all other investigated organs, the uptake was similar for both injected amounts. However, in the end, better tumor-to-background ratios were obtained when sub-equimolar amounts of drug relative to MSA were injected. This is an important finding for future SPECT imaging studies with c.a. [^{97}Ru]BOLD-100 that bear the potential of clinical application, for example, in patient stratification. In the future, the production and target workup of ^{97}Ru needs to be improved, as well as the radiochemical yield for the synthesis of c.a. [^{97}Ru]BOLD-100. To identify the best protocol for preclinical SPECT imaging studies, tissue distribution experiments with doses of radiolabeled BOLD-100 even lower than herein reported are planned and will be reported in due time.

4. Experimental part

Materials and methods

All solvents were purchased from commercial sources and used without any further purification. Millipore water (Milli Q® 8/16 Direct System, Merck), acetonitrile (ACN, for HPLC, gradient grade ≥99%, Sigma-Aldrich), and trifluoroacetic acid (TFA, Sigma Aldrich) were used for HPLC. Ru foil (99.9%, Goodfellow), Mo foil (99.9%, Goodfellow), ruthenium(III) chloride hydrate (Johnson Matthey), hydrogen peroxide (reagent grade, 30%), ion exchange resin Dowex® 1-X8 (Sigma Aldrich), hydrochloric acid (37%, VWR & p.a., Carl Roth), sodium hydroxide (p.a., Merck), sodium hypochlorite (12% Cl, technical grade, Carl Roth), acetonitrile (ACN; VWR), ethanol (absolute, EMPROVE® exp Ph Eur, BP, JP, USP, Merck), methyl *tert*-butyl ether (MTBE; anhydrous 99.8%, Sigma Aldrich), indazole (Polivalent-95), cesium chloride (99+% pure, Acros Organics), sodium sulfate (99% extra pure, anhydrous, Acros Organics), aluminum sulfate octadecahydrate (98+%, extra pure, Acros Organics) were used for the target work up and syntheses. All solutions of chemicals were prepared shortly before use.

Gamma-ray spectrometry measurements for ^{97}Ru (at the Arronax facility) were performed using a high-purity germanium (HPGe) detector (Canberra, France). Calibration of the detector in energy and efficiency was implemented with ^{57}Co, ^{60}Co, and ^{152}Eu calibrated sources from LEA-CERCA (France). The spectra were recorded with the LVis software from Ortec®.

Inductively coupled plasma optical emission spectroscopy (ICP-OES) measurements were performed on an ICP-OES XP Pro DUO from Thermo Fisher.

Gamma-ray spectrometry measurements for ^{103}Ru were performed using a high-purity germanium (HPGe) detector (ORTEC) connected to a loss free counting module. Efficiency calibration of the detector was performed by calibration solution with certified activities of ^{241}Am, ^{109}Cd, ^{57}Co, ^{139}Ce, ^{203}Hg, ^{113}Sn, ^{85}Sr, ^{137}Cs, ^{88}Y and ^{60}Co (Eckert & Ziegler). Spectra were recorded and evaluated using Genie2k software.

HPLC analysis was performed with a Chromolith® performance RP-18e 100_4.6 mm column (Merck) on a Merck Hitachi L-6200A intelligent pump with a Merck Hitachi UV detector L-7400 and a Packard Radiomatic Flo-One Beta detector equipped with a bismuth germanium oxide (BGO) cell for radioactivity detection in serial arrangement. For analysis, a gradient was applied using acetonitrile with 0.1% TFA (solvent A) and Milli Q water with 0.1% TFA (solvent B): 0–3 min, 10% A; 3–14 min, 55% A; 14–16 min, 95% A; 16–19.5 min, 95% A; 19.5–21 min, 10% A; 21–22 min,10% A (A + B = 100%, flowrate = 3 mL min^{-1}, total run time = 22 min, UV wavelength = 220 nm). All samples were filtered through a 0.22 μm filter (Millex®-GV) before injection.

The radioactivity of the samples was measured on a VDC–405 dose calibrator V3.26. Calibration was performed with the delivered ruthenium solutions and conversion factors were determined using ^{99m}Tc settings for ^{97}Ru (factor 360) and ^{137}Cs settings for ^{103}Ru (factor 0.915). For centrifugation during synthesis a Fisherbrand™ Mini-Centrifuge from Fisher Scientific was used (max. 2000*g*, 5–30 s.). Organ samples were measured on PerkinElmer Wizard^2 gamma counter. A microcryotome (Microm HM 560, HistoCom) from Thermo Scientific (Wiener Neudorf, Austria) was used for the cryo-cutting of tumors, which were fixed with Tissue-Tek® (O.C.T.™ compound, Sakura Finetek Europe) on superfrost slices from Thermo Scientific (Menzel-Gläser SUPERFROST® PLUS, microscope slides, Braunschweig, Germany). The Cyclone phosphor imager (Cyclone Plus storage phosphor system) and phosphor imaging plates (Multisensitive phosphor screens long type MS, PPN7001724) were purchased from PerkinElmer (Corporate Headquarters, Waltham, Massachusetts, USA), and lead shielded cassettes (Fisher Biotech Autoradiography Cassette FBCS 1417) from Fisher Scientific (Pittsburgh, USA). Image analysis was performed with the OptiQuant® data processing software Version 5.0.

Radionuclide production

^{97}Ru. A foil of ^{nat}Mo with a thickness of 75 μm and a diameter of 20 mm (approximately 250 mg) was placed in a home-made target system between the α-particle beam and a water-cooled aluminum nose of the target. Alpha particles were extracted from a cyclotron with 67.4 MeV and sent in vault A2 at the Arronax facility (Saint-Herblain, France), which is equipped with a carbon degrader that allows reduction of the α-particle energy to 26 MeV on the Mo target foil. The intensity on the target was 15 μA and irradiation was performed for approximately 10 h, yielding 310 MBq at the EOI. After the irradiation, the Mo foil was dissolved in 15 mL of H_2O_2 (30%) at 70 °C. The solution was loaded onto an ion exchange column, packed with Dowex® 1-X8 resin (3.7 g). ^{97}Ru was eluted with 25 mL of H_2O_2 (30%) and directly loaded onto a second column packed with Dowex® 1-X8 (3.7 g of resin). After the elution of ^{97}Ru with 35 mL of H_2O_2, the solution was evap-

orated to dryness, and recovered in 0.8–1.7 mL of HCl (8 M), yielding deliverable activities of 74–106 MBq mL^{-1} (0.2–0.3 GBq/nmol). The total amount of Mo and Ru in the final solution was determined by ICP-OES (0.5–2.5 mg L^{-1} Mo and 31.7–36.6 μg L^{-1} Ru) and the radiochemical yield of ^{97}Ru was 40–56%. Radioactive impurities of ^{95}Ru ($t_{1/2}$ = 1.6 h), ^{95m}Tc ($t_{1/2}$ = 61 d) and ^{95}Tc ($t_{1/2}$ = 20.0 h) were observed (ESI, Fig. S1†). For the synthesis of radiolabeled BOLD-100, $^{nat}RuCl_3$ was added as a carrier to enable isolation of intermediates and the final product.

^{103}Ru. Pieces of 6.6 mg and 4.2 mg 1 mm thick ^{nat}Ru metal foil were enclosed in quartz ampoules under 500 mbar helium for improved cooling and to prevent radiation-enhanced oxidation during irradiation. The samples were irradiated in the high flux position V4 of the high flux reactor of Institut Laue-Langevin (Grenoble, France) in a thermal neutron flux of about 5×10^{14} n cm^{-2} s^{-1} for 6.0 days and with a flux of 1×10^{15} n cm^{-2} s^{-1} for 8.2 days. After the decay of short-lived radionuclides (^{105}Ru, ^{105}Rh, and ^{97}Ru), the target material was processed further (CLIP, Vienna). The activity at the EOI was 643–1049 MBq (9.8–25.2 MBq μmol^{-1}).

The irradiated capsule was opened 15 days and 119 days after irradiation and the ^{103}Ru metal (78.5–805 MBq) was transferred into a conical 5 mL vial with a Teflon septum and a stirring bar. Sodium hydroxide (0.35 M, 200 μL) and sodium hypochlorite (12% Cl, 150 μL) were added, and the reaction mixture was stirred at room temperature for 24 h, resulting in a color change from colorless to dark reddish brown of the solution. The mixture was quenched by the addition of HCl (37%, 2.5 mL), which caused precipitation of NaCl as a granular solid. Activity measurements indicated no loss of ^{103}Ru. After 120 min, a perfluoroalkoxy alkane (PFA) tubing was inserted through the septum, and the dark red solution was transferred into a shielded receiver flask by application of negative pressure. This procedure yielded 64.7–648.2 MBq of c.a. ^{103}Ru (81–82% radiochemical yield) in a total volume of 2.6–3.0 mL and a radionuclide purity >99.9% (determined by gamma ray spectroscopy, ESI, Fig. S2†). The molar activity after the target workup was 1.2–19.4 MBq μmol^{-1}.

Syntheses

[^{97}Ru]KP1019 ([^{97}Ru]indazolium *trans*-[tetrachloridobis(indazole)ruthenate(III)]) (1a). $RuCl_3 \cdot xH_2O$ (6 mg, 29 μmol, 1 eq.) was dissolved in 0.5 mL conc. HCl (37%) and ethanol (1 mL). 0.5 mL of the ^{97}Ru-solution (18 ng Ru, 6.3 MBq, in HCl, 8 M) was added, and the mixture was refluxed for 3 h. Indazole (23 mg, 192 μmol, 6.64 eq.) dissolved in H_2O (0.1 mL) and conc. HCl (37%, 0.4 mL) was added to the ruthenium solution. The reaction mixture was refluxed for 3 h. After cooling to RT, the formed suspension was centrifuged, and the supernatant was removed. The remaining solid was washed three times with 2 M HCl (1 mL). The obtained product (10 mg, 61%, 3.1 MBq; yields were determined henceforth by the ratio of isolated radioactivity to starting radioactivity) was analyzed using HPLC.

HPLC: t_R ($Hind^+$) = 5.17 min, t_R ([^{97}Ru][$Ru(ind)_2Cl_4$]$^-$) = 7.56 min (UV), 7.81 min (radiochannel).

Radiochemical yield (RCY): 61%.

Radiochemical purity (RCP): >99%.

[^{97}Ru]Cesium *trans*-[tetrachloridobis(indazole)ruthenate(III)] (2a). Indazolium salt **1a** (11 mg, 18 μmol) was suspended in ethanol (0.75 mL), CsCl (14 mg, 81 μmol, 2.8 eq.) was added and the mixture was stirred at RT for 2 h. The solid was separated by centrifugation, washed twice with ethanol (0.5 mL), and stirred in a 2 : 1 v/v ethanol water mixture (0.75 mL) for 15 min at RT. The product (10 mg, 55%, 2.7 MBq) was centrifuged, washed twice with ethanol (0.5 mL), and analyzed using HPLC.

HPLC: t_R ([^{97}Ru][$Ru(ind)_2Cl_4$]$^-$) = 7.36 min (UV), 7.64 min (radiochannel).

RCY: 55%.

RCP: >99%.

[^{97}Ru]BOLD-100 ([^{97}Ru]sodium *trans*-[tetrachloridobis(indazole)ruthenate(III)]) (3a). Cesium salt **2a** (10 mg, 16 μmol) was suspended in a solution of $NaAl(SO_4)_2 \cdot 18H_2O$ (1.1 M, 1 mL), CsCl (spatula tip, catalytic amount) was added, and the mixture was stirred at RT for 24 h. The crude solid product was obtained by centrifugation and washing with a saturated Na_2SO_4 solution. The obtained moist solid was stirred in ACN (0.5 mL) for 15 min at RT. The suspension was centrifuged and washed with ACN (two times, 0.5 mL). The filtrates were combined, diluted with MTBE (5 : 1), and set aside for 1 h. The precipitated brown needles were collected by centrifugation, washed with MTBE, and dried on air to yield pure c.a. [^{97}Ru]BOLD-100 (1.2 mg, overall radiochemical yield: 0.2 MBq, 8%; overall chemical yield determined by weighing the substance: 1.9 mg, 13%).

HPLC: t_R ([^{97}Ru][$Ru(ind)_2Cl_4$]$^-$) = 7.03 min (UV), 7.45 min (radiochannel).

RCY: 8%; overall chemical yield: 13%.

RCP: >99%.

All chromatograms can be found in the ESI (Fig. S3–S8†). The synthetic procedure (**1b–3b**) of c.a. [^{103}Ru]BOLD-100 (**3b**) can be found in the ESI and was performed as published earlier.[34]

Animals

Female Balb/c mice were purchased from Envigo (San Pietro al Natisone, Italy). The animals were kept in a pathogen-free environment and every procedure was done in a laminar airflow cabinet. The experiments were performed according to the regulations of the Ethics Committee for the Care and Use of Laboratory Animals at the Medical University Vienna (ethic number BMWF-66.009/0394-V/3b/2018), the U.S. Public Health Service Policy on Human Care and Use of Laboratory Animals as well as the United Kingdom Coordinating Committee on Cancer Prevention Research's Guidelines for the Welfare of Animals in Experimental Neoplasia.

For an evaluation of organ distribution, CT26 cells (5×10^5 in serum-free medium) were injected subcutaneously into the right flank of Balb/c mice. The animals were controlled for dis-

tress development every day and tumor size was assessed regularly by caliper measurement. CT26 cells were inoculated 10 days prior to drug application. Tumor volume was calculated using the formula: (length × width^2) and tumors reached a size of approx. 500 mm^3. Animals (14–18 weeks old) were treated once by intravenous tail-vein injection of **3b** at a dose of 3 or 30 mg kg^{-1} (dissolved in 0.9% NaCl, 0.6 mg per 100 μL per 20 g mouse or 0.06 mg per 100 μL per 20 g mouse) and a specific activity of 0.76–3.80 MBq mg^{-1}. The mice were anesthetized and sacrificed by cervical fracture 4, 24, 48, and 72 h p.i., with $n \geq 4$ for each time point. Samples of tumor, liver, kidneys, muscle, heart, lung, spleen, pancreas, stomach, colon, small intestine, brain, bone, and blood were collected from each mouse. For some mice ($n = 4$), blood was collected 5 min and 30 min p.i. *via* the facial vein. After clotting at RT, serum was isolated from the collected blood samples by centrifugation at 3000 rpm for 2 × 10 min and stored together with the collected tissue samples at −20 °C. Finally, the ruthenium content was determined *via* gamma counting.

Autoradiography

Snap-frozen tumor tissue samples were stored at −80 °C until further proceeding. Tumor samples were stored at −20 °C for 24 h, embedded in mounting medium, and cut into 20 μm thick tissue sections. Cryosections were mounted on adhesion slides, imaged with phosphor imager plates in lead shielded cassettes for up to 5 days, and analyzed with a Cyclone phosphor imager.

Conflicts of interest

There are no conflicts to declare.

Acknowledgements

The authors acknowledge Stefanie Marie Ponti, Anna Sophia Zacher (Preclinical Imaging Laboratory team, Medical University of Vienna), and Gerhard Zeitler (Center for Cancer Research, Medical University of Vienna) for technical support with the animal experiments. P. Heffeter was funded by the Fellinger Krebsforschungs Fonds. The cyclotron Arronax is supported by CNRS, Inserm, the Nantes University, the Regional Council of Pays de la Loire, local authorities, the French Government, and the European Union. Open Access Funding was provided by the University of Vienna.

References

1 R. C. Lange, R. P. Spencer and H. C. Harder, The antitumor agent *cis*-Pt$(NH_3)_2Cl_2$: distribution studies and dose calculations for ^{193m}Pt and ^{195m}Pt, *J. Nucl. Med.*, 1973, **14**, 191–195.

2 R. Trondl, P. Heffeter, C. R. Kowol, M. A. Jakupec, W. Berger and B. K. Keppler, NKP-1339, the first ruthenium-based anticancer drug on the edge to clinical application, *Chem. Sci.*, 2014, **5**, 2925–2932.

3 D. Kreutz, C. Gerner and S. M. Meier-Menches, in *Metal-based Anticancer Agents*, ed. A. Casini, A. Vessières and S. M. Meier-Menches, The Royal Society of Chemistry, London, 2019, 10, 246–270.

4 O. Dömötör, C. G. Hartinger, A. K. Bytzek, T. Kiss, B. K. Keppler and E. A. Enyedy, Characterization of the binding sites of the anticancer ruthenium(III) complexes KP1019 and KP1339 on human serum albumin via competition studies, *JBIC, J. Biol. Inorg. Chem.*, 2012, **18**, 9–17.

5 A. Bijelic, S. Theiner, B. K. Keppler and A. Rompel, X-ray Structure Analysis of Indazolium *trans*-[Tetrachlorobis(1*H*-indazole)ruthenate(III)] (KP1019) Bound to Human Serum Albumin Reveals Two Ruthenium Binding Sites and Provides Insights into the Drug Binding Mechanism, *J. Med. Chem.*, 2016, **59**, 5894–5903.

6 S. M. Meier-Menches, C. Gerner, W. Berger, C. G. Hartinger and B. K. Keppler, Structure–activity relationships for ruthenium and osmium anticancer agents–towards clinical development, *Chem. Soc. Rev.*, 2018, **47**, 909–928.

7 E. Reisner, V. B. Arion, B. K. Keppler and A. J. Pombeiro, Electron-transfer activated metal-based anticancer drugs, *Inorg. Chim. Acta*, 2008, **361**, 1569–1583.

8 H. Yin, L. Liao and J. Fang, Enhanced permeability and retention (EPR) effect based tumor targeting: the concept, application and prospect, *JSM Clin. Oncol. Res.*, 2014, **2**, 1010.

9 F. Kratz, Albumin as a drug carrier: design of prodrugs, drug conjugates and nanoparticles, *J. Controlled Release*, 2008, **132**, 171–183.

10 B. Schoenhacker-Alte, T. Mohr, C. Pirker, K. Kryeziu, P.-S. Kuhn, A. Buck, T. Hofmann, C. Gerner, G. Hermann, G. Koellensperger, B. K. Keppler, W. Berger and P. Heffeter, Sensitivity towards the GRP78 inhibitor KP1339/IT-139 is characterized by apoptosis induction via caspase 8 upon disruption of ER homeostasis, *Cancer Lett.*, 2017, **404**, 79–88.

11 S. J. Bakewell, D. F. Rangel, D. P. Ha, J. Sethuraman, R. Crouse, E. Hadley, T. L. Costich, X. Zhou, P. Nichols and A. S. Lee, Suppression of stress induction of the 78-kilodalton glucose regulated protein (GRP78) in cancer by IT-139, an anti-tumor ruthenium small molecule inhibitor, *Oncotarget*, 2018, **9**, 29698–29714.

12 S. Kapitza, M. Pongratz, M. A. Jakupec, P. Heffeter, W. Berger, L. Lackinger, B. K. Keppler and B. Marian, Heterocyclic complexes of ruthenium(III) induce apoptosis in colorectal carcinoma cells, *J. Cancer Res. Clin. Oncol.*, 2004, **131**, 101–110.

13 E. Schreiber-Brynzak, E. Klapproth, C. Unger, I. Lichtscheidl-Schultz, S. Göschl, S. Schweighofer, R. Trondl, H. Dolznig, M. A. Jakupec and B. K. Keppler, Three-dimensional and co-culture models for preclinical evaluation of metal-based anticancer drugs, *Invest. New Drugs*, 2015, **33**, 835–847.

14 P. Heffeter, K. Böck, B. Atil, M. A. Reza-Hoda, W. Körner, C. Bartel, U. Jungwirth, B. K. Keppler, M. Micksche,

W. Berger and G. Koellensperger, Intracellular protein binding patterns of the anticancer ruthenium drugs KP1019 and KP1339, *JBIC, J. Biol. Inorg. Chem.*, 2010, **15**, 737–748.

15 L. S. Flocke, R. Trondl, M. A. Jakupec and B. K. Keppler, Molecular mode of action of NKP-1339—a clinically investigated ruthenium-based drug–involves ER-and ROS-related effects in colon carcinoma cell lines, *Invest. New Drugs*, 2016, **34**, 261–268.

16 D. Wernitznig, K. Kiakos, G. Del Favero, N. Harrer, H. Machat, A. Osswald, M. A. Jakupec, A. Wernitznig, W. Sommergruber and B. K. Keppler, First-in-class ruthenium anticancer drug (KP1339/IT-139) induces an immunogenic cell death signature in colorectal spheroids *in vitro*, *Metallomics*, 2019, **11**, 1044–1048.

17 D. Baier, B. Schoenhacker-Alte, M. Rusz, C. Pirker, T. Mohr, T. Mendrina, D. Kirchhofer, S. M. Meier-Menches, K. Hohenwallner and M. Schaier, The anticancer ruthenium compound BOLD-100 targets glycolysis and generates a metabolic vulnerability towards glucose deprivation, *Pharmaceutics*, 2022, **14**, 238.

18 H. A. Herrmann, M. Rusz, D. Baier, M. A. Jakupec, B. K. Keppler, W. Berger, G. Koellensperger and J. Zanghellini, Thermodynamic genome-scale metabolic modeling of metallodrug resistance in colorectal cancer, *Cancers*, 2021, **13**, 4130.

19 B. Neuditschko, A. A. Legin, D. Baier, A. Schintlmeister, S. Reipert, M. Wagner, B. K. Keppler, W. Berger, S. M. Meier-Menches and C. Gerner, Interaction with Ribosomal Proteins Accompanies Stress Induction of the Anticancer Metallodrug BOLD–100/KP1339 in the Endoplasmic Reticulum, *Angew. Chem., Int. Ed.*, 2021, **60**, 5063–5068.

20 H. A. Burris, S. Bakewell, J. C. Bendell, J. Infante, S. F. Jones, D. R. Spigel, G. J. Weiss, R. K. Ramanathan, A. Ogden and D. Von Hoff, Safety and activity of IT-139, a ruthenium-based compound, in patients with advanced solid tumours: a first-in-human, open-label, dose-escalation phase I study with expansion cohort, *ESMO Open*, 2016, **1**, e000154.

21 **https://clinicaltrials.gov/**, (accessed 7.12.2023).

22 G. M. O'Kane, J. L. Spratlin, D.-Y. Oh, S. Y. Rha, E. Elimova, P. Kavan, M. K. Choi, R. A. Goodwin, S. T. Kim, D.-H. Koo, K. Halani, E. R. McAllister, M. Jones, M. Snow, Y. Lemmerick, G. Spera and J. Pankovich, BOLD-100-001 (TRIO039): A phase 1b/2a study of BOLD-100 in combination with FOLFOX chemotherapy in patients with pretreated advanced gastric and biliary tract cancer: Efficacy and safety analysis, *J. Clin. Oncol.*, 2023, **41**(16_suppl 2023 ASCO Annual Meeting), 4098–4098.

23 J. Spratlin, G. O'Kane, D.-Y. Oh, S. Y. Rha, E. McWhirter, E. Elimova, P. Kavan, M. K. Choi, D. W. Kim, R. Goodwin, J. R. Hecht, S. T. Kim, D.-H. Koo, K. Halani, E. R. McAllister, M. Jones, M. Snow, Y. Lemmerick, G. Spera and J. Pankovich, BOLD-100–001 (TRIO039): A phase 1b/2a dose-escalation study of BOLD-100 in combination with FOLFOX chemotherapy in patients with pretreated advanced colorectal cancer: interim efficacy, safety and tolerability analysis, *Cancer Res.*, 2023, **83**(8_Supplement), CT149.

24 G. Subramanian and J. G. McAfee, 97Ru: Preliminary Evaluation of a New Radionucide for Use in Nuclear Medcine, *J. Nucl. Med.*, 1970, **11**, 365.

25 S. Srivastava, P. Richards, A. Brill, Z. Oster, P. Som, M. Gil, R. Fairchild, A. Goldman, E. Schachner and D. Sacker, Ruthenium-97 DTPA: a new radiopharmaceutical for cisternography, *J. Nucl. Med.*, 1981, **22**, 269–273.

26 K. Krane, Neutron capture by Ru: Neutron cross sections of 96,102,104Ru and γ-ray spectroscopy in the decays of 97,103,105Ru, *Phys. Rev. C*, 2010, **81**, 044310.

27 K. Shibata, Evaluation of neutron nuclear data on ruthenium isotopes, *J. Nucl. Sci. Techol.*, 2013, **50**, 1177–1187.

28 F. Tárkányi, A. Hermanne, F. Ditrói, S. Takács and A. Ignatyuk, Investigation of activation cross section data of alpha particle induced nuclear reaction on molybdenum up to 40 MeV: Review of production routes of medically relevant ^{97,103}Ru, *Nucl. Instrum. Methods Phys. Res., Sect. B*, 2017, **399**, 83–100.

29 M. Sitarz, E. Nigron, A. Guertin, F. Haddad and T. Matulewicz, New Cross-Sections for natMo(α,x) Reactions and Medical 97Ru Production Estimations with Radionuclide Yield Calculator, *Instruments*, 2019, **3**, 7.

30 N. Zaitseva, E. Rurarz, M. Vobecky, K. Hwan, K. Nowak, T. Thétal, V. Khalkin and L. Popinenkova, Excitation Function and Yield for ^{97}Ru Production in ^{99}Tc(p,3n)^{97}Ru Reaction in 20–100 MeV Proton Energy Range, *Radiochim. Acta*, 1992, **56**, 59–68.

31 M. Neves, A. Kling and A. Oliveira, Radionuclides used for therapy and suggestion for new candidates, *J. Radioanal. Nucl. Chem.*, 2005, **266**, 377–384.

32 M. Brandt, J. Cardinale, M. L. Aulsebrook, G. Gasser and T. L. Mindt, An overview of PET radiochemistry, part 2: Radiometals, *J. Nucl. Med.*, 2018, **59**, 1500–1506.

33 **https://www-nds.iaea.org/**, (accessed 05.11.2023).

34 B. Happl, M. Brandt, T. Balber, K. Benčurová, Z. Talip, A. Voegele, P. Heffeter, W. Kandioller, N. P. Van der Meulen and M. Mitterhauser, Synthesis and Preclinical Evaluation of Radiolabeled [103Ru]BOLD-100, *Pharmaceutics*, 2023, **15**, 2626.

35 J. Zaias, M. Mineau, C. Cray, D. Yoon and N. H. Altman, Reference values for serum proteins of common laboratory rodent strains, *J. Am. Assoc. Lab. Anim. Sci.*, 2009, **48**, 387–390.

36 M. Sulyok, S. Hann, C. Hartinger, B. Keppler, G. Stingeder and G. Koellensperger, Two dimensional separation schemes for investigation of the interaction of an anticancer ruthenium(III) compound with plasma proteins, *J. Anal. At. Spectrom.*, 2005, **20**, 856–863.

37 W. P. Griffith, *The chemistry of the rarer platinum metals (Os, Ru, Ir, and Rh)*, Interscience publishers, New York, 1967.

38 F. J. Dixon, P. H. Maurer and M. P. Deichmiller, Half-lives of homologous serum albumins in several species, *Proc. Soc. Exp. Biol. Med.*, 1953, **83**, 287–288.

39 G. H. Heppner, Tumor heterogeneity, *Cancer Res.*, 1984, **44**, 2259–2265.
40 A. Marusyk and K. Polyak, Tumor heterogeneity: causes and consequences, *Biochim. Biophys. Acta, Rev. Cancer*, 2010, **1805**, 105–117.
41 I. O. Umeda, K. Tani, K. Tsuda, M. Kobayashi, M. Ogata, S. Kimura, M. Yoshimoto, S. Kojima, K. Moribe and K. Yamamoto, High resolution SPECT imaging for visualization of intratumoral heterogeneity using a SPECT/CT scanner dedicated for small animal imaging, *Ann. Nucl. Med.*, 2012, **26**, 67–76.
42 S. Kuznetsov, L. Snopova, M. Karabut, M. Sirotkina, N. Buyanova, T. Kalganova, V. Elagin, I. Senina-Volzhskaya, L. Barbashova and A. Shumilova, Features of morphological changes in experimental CT-26 tumors growth, *Mod. Technol. Med.*, 2015, **7**, 32–37.